Severely Noisy Image Segmentation via Wavelet Shrinkage Using PSO and Fuzzy C-Means

Saeed Mirghasemi, Peter Andreae, Mengjie Zhang, Ramesh Rayudu
School of Engineering and Computer Science
Victoria University of Wellington, Wellington, New Zealand
Email: {saeed.mirghasemi, peter.andreae, mengjie.zhang, ramesh.rayudu}@ecs.vuw.ac.nz

***Abstract*—The necessity of proposing algorithms that are effective in noisy image segmentation is clear in many real-world applications. This paper proposes a new algorithm for severely noisy image segmentation by looking at the proper choice of feature, and feature manipulation. We are using Discrete Wavelet Transformation (DWT) as a tool to provide our method with the proper feature, and then we manipulate it via wavelet shrinkage. Particle Swarm Optimization (PSO) is used to adaptively search for threshold values that produce the best segmentation results when applied in the wavelet shrinkage, and Fuzzy C-Means (FCM) is used as a fitness metric in PSO. The proposed method was tested on two different datasets being extremely contaminated with the common Gaussian noise. These tests indicate the superior performance and consistency of the proposed method in comparison to other state-of-the-art methods.**

I. Introduction

Image segmentation is considered one of the foremost mid-level steps in image processing applications like image compression [1], image recognition [2], traffic control and surveillance [3], object detection [4], and many more. It is a procedure of partitioning an image into disjoint regions that are homogeneous in intensity, color, or texture. Among the applications of image segmentation, there are domains where segmentation needs to be done on noisy images. Noise could be added to images via capturing or transmission procedures. For instance, medical images suffer from intensity inhomogeneities and noise. Also, natural images have additive Gaussian noise. Another field that needs methods handling noisy images is remote image analysis with applications in Synthetic Aperture Radar [5], and satellite [6] image processing.

Fuzzy C-Means (FCM) as a fuzzy clustering algorithm has the potential to deal with both problems of image segmentation and noise removal at the same time. However, a common issue in applying FCM to image data is determining how to include spatial information in clustering along with other information such as intensity or color. In recent years, many FCM-based algorithms have been proposed to deal with the problem of noisy image segmentation [7], [8], [9], [10], [11], [12], [13], [14]. Most of these algorithms modify the objective function of the original FCM to have more spatial information included from a surrounding window around each pixel. Some of these algorithms are parameter dependent [7], [8], [9], [10] which requires prior information about the type and volume of noise.

One technique of recent interest that can deliver accurate segmentation results, when merged with FCM-based algorithms, is Particle Swarm Optimization (PSO). It is extensively used in optimization problems [15], [16], and is gaining popularity in the field of noisy image segmentation with the definitive contribution still to be made.

A. Goals

This paper proposes a new FCM-based noisy image segmentation method using PSO and wavelet transform. The algorithm requires no parameter tuning for the volume of noise, and shows stable and accurate results on different images with different noise volumes. While there has been much research on changing the objective function of FCM [7], [8], [9], [10], [11], [12], or new similarity metrics for FCM [13], [14] to improve the performance, there has not been a stress on the importance of feature choice and manipulation in the literature. This paper targets the problem from the feature analysis point of view. It explores the potentials of PSO and wavelet-based thresholding for noisy image segmentation. We demonstrate the effect of appropriate choice of features and feature processing on FCM performance with superior results compared to other state-of-the-art methods.

II. Background

A. Fuzzy C-Means and the Related Algorithms

Fuzzy C-Means (FCM) was first introduced in [17], and then extended in [18] by Bezdek. It is a clustering algorithm in which all the datapoints are considered to belong to all the clusters to some extent. Datapoints (pixels in our application), are represented as a set, $X = \{x_1, x_2, ..., x_N\}$, where a p-dimensional vector as features is associated to each pixel, x_i. The aim is to find C cluster centers in a way that the following objective function is minimized:

$$J = \sum_{i=1}^{N} \sum_{j=1}^{C} u_{ij}^{m} d^2(x_i, v_j) \tag{1}$$

where N and C are the number of pixels and clusters respectively, u_{ij} is a value specifying the degree of membership of pixel i to cluster j which needs to satisfy: $u_{ij} \in [0,1]$ and $\sum_{j=1}^{C} u_{ij} = 1$, and m is the weighting exponent. $d(.,.)$ is the distance metric, and $d(x_i, v_j)$ is the distance between pixel x_i and cluster centre v_j which uses the Euclidean metric in our approach. Using Lagrange multipliers

the two following updating equations are obtained which are necessary but not enough to have Eq. (1) at its minimum:

$$v_j^k = \frac{\sum_{i=1}^{N} \left(u_{ij}^k\right)^m x_i}{\sum_{i=1}^{N} \left(u_{ij}^k\right)^m} \quad (2) \qquad u_{ji}^{k+1} = \frac{1}{\sum_{l=1}^{C} \left(\frac{d(x_i, v_j^k)}{d(x_i, v_l^k)}\right)^{2/m-1}} \quad (3)$$

The traditional applications of FCM to image segmentation fail to produce accurate noisy segmentation results as the objective function did not consider any spatial information. In this manner, the first notable attempt to overcome this weakness is [7] known as FCM_S. The method was proposed to conquer the intensity inhomogeneities present in the segmentation of MRI images by allowing the labeling of a pixel to be affected by its immediate neighborhood. Since FCM_S was computationally expensive, FCM_S1 and FCM_S2 were proposed [8] to improve both efficiency and effectiveness by using a pre-calculated mean and median filtration of the surrounding window for FCM_S1 and FCM_S2 respectively. EnFCM was proposed [9] as another modification of FCM. It uses a linearly weighted filter applied to the noisy image, and then FCM is performed on the intensity histogram of the image. The algorithms mentioned so far have a tuning parameter, termed α, which has to be large enough to suppress the effect of noise, and has to be small enough to preserve the details in an image. Since these methods are parameter dependent, their utilization was narrowed down to certain types and volumes of noise. FGFCM [10] was therefore proposed later to reduce the parameter dependency of the former modifications. FGFCM proposes a non-linear filtering factor which still has two tuning parameters termed as λ_s and λ_g, but it was shown that the dependency of FGFCM to these parameters is much less than that of the previous methods to α. Motivated by the strengths of all the previous methods, the parameter-free FLICM was proposed [11]. A new fuzzy factor was introduced into the objective function that considers gray and spatial information simultaneously. Although the method is parameter-free and performs better than its predecessors, the segmentation results are not accurate in the case of multi-intensity noisy images [19]. Also, FLICM is problematic when it comes to identifying the class of boundary pixels [12], and severely noisy image segmentation.

B. Wavelets

Wavelet transform is a technique which provides multi-resolution representations for image analysis [20]. One of the primary properties of wavelet transforms is its sparsity when applied to real-world signals. This means that they contain a few large coefficients encompassing the majority of the energy of the signal. The rest are unimportant coefficients that carry no significant information. This feature of wavelets is quite favorable for image denoising. To apply wavelet decomposition on an image, 2-dimensional Discrete Wavelet Transform (2D-DWT) is required to be done by applying 1D-DWT along the rows, and then the columns of an image. After applying 2D-DWT on an image, it is decomposed into four sub-bands. These four sub-bands are the results of applying high-pass and low-pass filters in vertical and horizontal directions, and are named HH1, LH1, HL1, and LL1, or diagonal, horizontal, vertical and approximation coefficients respectively. LL1 can be further decomposed to give another set of coefficients at the second scale (Fig. 1-b).

Applying 2D-DWT to an image $f(x,y)$ of size $M \times N$ is performed according to the block diagram provided in Fig. 1-a, using the following formulas:

$$W_\varphi(j_0,m,n) = \frac{1}{\sqrt{MN}} \sum_{x=0}^{M-1} \sum_{y=0}^{N-1} f(x,y) \varphi_{j_0,m,n}(x,y)$$

$$W_\psi(j,m,n) = \frac{1}{\sqrt{MN}} \sum_{x=0}^{M-1} \sum_{y=0}^{N-1} f(x,y) \psi^i_{j,m,n}(x,y), i = \{H,V,D\} \quad (4)$$

in which j_0 is an arbitrary starting scale, and the $W_\psi(j,m,n)$ coefficients define an approximation of $f(x,y)$ at scale j_0. The $W_\psi(j,m,n)$ coefficients add horizontal, vertical, and diagonal details for scales $j \geqslant j_0$.

Thresholding wavelet coefficients can suppress the effect of noise [21], but it is a difficult task to determine the appropriate threshold values. Under-thresholding leaves a lot of noise which causes many segmented regions in an image, while over-thresholding image deforms the boundary lines, and also causes redundant segmented regions around the edges. Generally, over-thresholding could also eliminate details from an image.

C. Particle Swarm Optimization

Particle Swarm Optimization (PSO) was introduced by Kennedy and Eberhart in 1995 [22], [23] motivated by social behaviors of organisms particularly choreography of bird flocking. Talking of PSO modus operandi, it starts with a swarm of potential solutions (population size) that are updated iteratively based on their position and velocity in the search space. Therefore, particle i, has position, x_i, and velocity, v_i. Knowing that the search space is D-dimensional, each particle is represented by $X_i = (x_{i1}, x_{i2} ... x_{iD})$ and $V_i = (v_{i1}, v_{i2}, ..., v_{iD})$ as arrays of the positions and velocities of each particle. The movement is done based on *pbest* which is the best previous position of a particle, and *gbest* which is the best position so far obtained in the search. Position and velocity of each particle are updated using:

$$v_{id}^{k+1} = \omega \times v_{id}^k + c_1 r_1 (pbest_{id} - x_{id}^k) + c_2 r_2 (gbest_d - x_{id}^k) \quad (5)$$

$$x_{id}^{k+1} = x_{id}^k + v_{id}^{k+1} \quad (6)$$

where k is the iteration in the search procedure, $d \in D$ is the dth dimension, ω is the inertia weight, c_1 and c_2 are constants, and r_1 and r_2 are random numbers in [0,1]. The goodness of each solution is determined through a fitness evaluation in each iteration, which is defined according to the application. PSO converges when a certain degree of accuracy is achieved or a fixed number of iterations is applied.

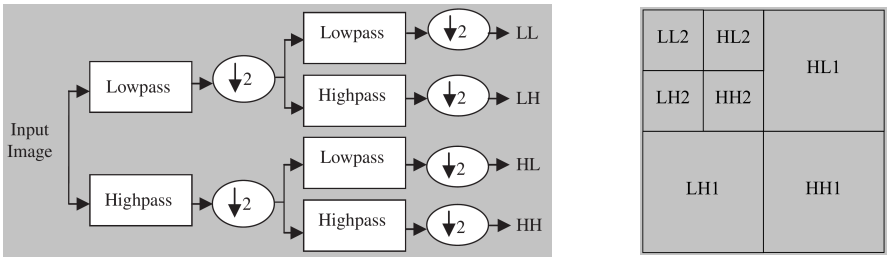

(a) (b)

Fig. 1: Two-dimensional DWT. (a) the analysis filter bank; (b) the resulting two-scale decomposition

D. Related Work

Two distinctive approaches are recognizable in the research history of using FCM or its modification alongside PSO for noisy image segmentation. The first approach contains methods that use PSO to look for cluster centers that optimizes an already existing FCM-based algorithm [24], [25], [26].

The second approach, a very recent trend, uses PSO to modify the distance metric used in FCM to calculate the distance between datapoints and cluster centers. For instance, a new similarity metric is proposed in [27] using wavelets as features for superpixels. The new similarity metric is tuned for parameters using PSO. Another case is the method proposed in [13], which is based on simple statistical features extracted from a surrounding window, and then including them along with fuzzy membership and intensity values into a new similarity metric. PSO was utilized to adaptively determine the contribution of each feature into noise removal according to the properties of each image. A similar work was also proposed entangling coordinates of the prototypes of each cluster with the corresponding feature associated with each pixel [14].

FCM-based noisy image segmentation approaches have some problems. Some of these approaches are parameter dependent, and some perform poorly on severely noisy images. In this paper, we introduce a new FCM-based noisy image segmentation algorithm which not only resolves the addressed problems, but also shows significant improvement compared to other algorithms.

III. The Proposed Method

This paper proposes a new algorithm for noisy image segmentation by adaptively thresholding wavelet coefficients utilizing PSO. The proposed method introduces a unique set of threshold values for each image according to noise volume, and properties of the image under consideration. FCM clustering takes part in both evaluating thresholding performances in PSO, and the final segmentation procedure. The idea is to firstly transform an image to wavelet domain using a specific wavelet function at a certain number of scales. Secondly, PSO searches for an optimal set of threshold values to threshold the wavelet coefficients obtained from the previous step. The outcome of the PSO search is then applied for a final denoising. Thirdly, the image is reconstructed with the thresholded coefficients to generate the denoised image. Lastly, FCM is used to cluster the reconstructed image, and segment it according to the mean intensity value of each cluster. Fig. 2 shows the block diagram of the proposed method.

A. PSO Representation

In our approach, PSO is utilized for wavelet coefficients manipulation and therefore better segmentation results. More specifically, PSO looks for the optimum values of the thresholds among different wavelet sub-bands at different scales. This gives the thresholding procedure the adaptivity of tuning the threshold values according to noise volume and image properties. Each particle thresholds vertical, horizontal, and diagonal coefficients of each scale with a different value. Knowing that there are three detail coefficients (or sub-bands) named as horizontal, vertical, and diagonal at each scale, there would be three threshold values for each scale of transformation. The wavelet transform is performed at five scales in our problem. Therefore, each particle is a set of potential threshold values in the form of a 15-dimensional array termed as $[\theta_1, \theta_2, ..., \theta_{15}]$. To prevent particles from under- and over-thresholding the coefficients, we set a minimum and a maximum value for each threshold value for better convergence of the PSO search. The minimum value is zero and the maximum value is obtained according to the Universal threshold proposed in Visu Shrink method [28]. The Universal threshold value is given by:

$$\theta_U = \sigma\sqrt{2\ln(n)} \tag{7}$$

where σ is the noise standard deviation, and n is the number of pixels in an image. Since σ is unknown in our case, it is obtained using a robust median estimator [28] from the finest scale of wavelet coefficients:

$$\sigma = \frac{median\left[|x_{ij} : i, j \in HH_1|\right]}{0.6745} \tag{8}$$

where x are noisy coefficients of sub-band HH_1.

Although the Universal threshold will thoroughly suppress the effect of noise, the value is bigger than necessary [29], and therefore over-smooths the underlying image.

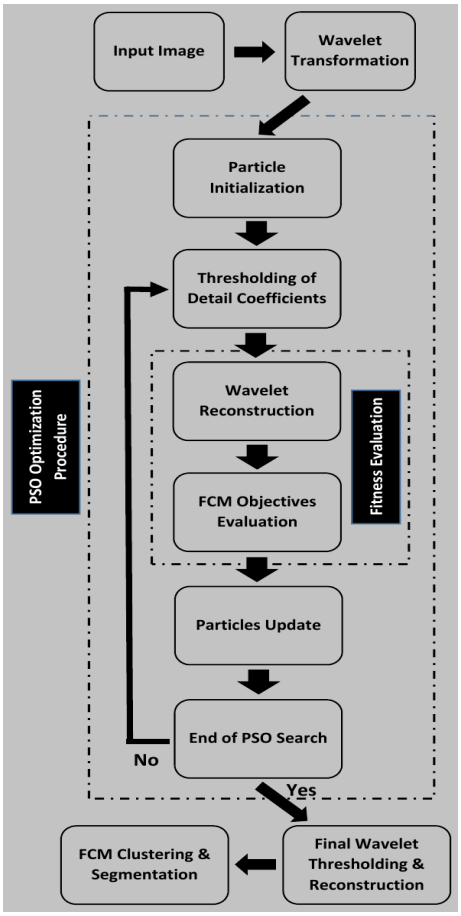

Fig. 2: Block diagram of the proposed method

B. Wavelet Transformation and Thresholding

As mentioned before thresholding based on wavelet coefficients is a difficult task because improper threshold values or number of scales may lead to imprecise and incorrect segmentation results. When thresholding wavelet coefficients, the threshold has to be large enough to attenuate the effect of noise, and it has to be small enough to preserve the details in an image. The same thing is ruling over the number of scales. If the number of scales is too low, both denoising and segmentation are not done properly, and if it is too large details will vanish from an image. Empirically, we have realized that thresholding wavelet coefficients at five scales has the potential to show suitable segmentation performances while keeping important details. The family of filters also play an important role in this manner. Different wavelet filters have different properties [30].

Each wavelet-based thresholding needs a thresholding function through which the wavelet coefficients are thresholded. The thresholding function determines the criterion under which we manipulate each coefficient for denoising purposes. In this paper, we have selected the simple and effective soft thresholding function [21]. The PSO-proposed threshold values are used within this function:

$$Y = \begin{cases} sign(X) \times (|X| - \theta), & \text{if } |X| > \theta \\ 0, & \text{if } |X| \leq \theta \end{cases} \tag{9}$$

where X is a wavelet coefficient and θ is a threshold value.

C. Fitness Evaluation

The thresholding performance of each particle needs evaluation in each iteration of PSO. For this, we perform a reverse wavelet transform on what is being left off of the thresholded coefficients to reconstruct the denoised image. The intensity values of each pixel form the reconstructed image are then used as features for FCM clustering. FCM clustering performance is then being used as the fitness metric in PSO. To measure the FCM clustering performance, FCM objective function introduced in Eq. 1 is calculated. Therefore, the FCM objective function acts as the fitness function for performance evaluation of particles. In each iteration of the search, potential solutions in the population are tested, and the best particle will be conveyed to the next iteration.

IV. Experiment Design

A. Datasets and Evaluation

To evaluate the proposed method comprehensively we test our method on two different image datasets. The first one is a Synthetic image dataset in which the images are composed of a limited number of regions, easily distinguishable due to the fact that each region has a single intensity value, and they are geometrically simple. Having said that, this dataset is helpful in giving an understanding of how our method performs when dealing with simply recognizable compact regions in an image. There are five images in this dataset named $S1, S2, ..., S5$. While performing FCM clustering on them, the number of clusters is set to 4, 3, 3, 4, and 3 respectively based on the number of regions provided in the original image.

The second dataset is taken from the well-known Berkeley dataset [31] specifically created for image segmentation and boundary detection. For this dataset, five images named 3096, 42049, 167062, 86016, 196027 have been selected for a similar experiment. The number of clusters has been pre-determined as 2, 2, 3, 2, and 2 respectively, based on the main compact regions in the image/groundtruth. Fig. 3 shows the original images of these two datasets. Then, each image is corrupted by Gaussian noise. The variance of noise ranges from 10% to 80% to explore the performance of our method as noise volume changes. For a quantitative evaluation, we use the Segmentation Accuracy (SA) [7]:

$$SA = \sum_{i=1}^{C} \frac{A_i \cap S_i}{\sum_{j=1}^{C} S_j} \tag{10}$$

in which A_i represents the number of segmented pixels belonging to the ith cluster in the segmented image, and S_i is the number of pixels belonging to the ith cluster in the ground truth image.

We have compared our method to several state-of-the-art FCM-based noisy image segmentation methods. These methods are FCM_S1 and FCM_S2 [8], EnFCM [9], FGFCM, FGFCM_S1 and FGFCM_S2 [10], and FLICM [11].

B. Parameter Design

PSO, FCM, and wavelet transformation all have parameters to set, and we have mentioned a few of them before. Table I shows the full set of parameters in the proposed algorithm and the values allocated to them in the experiments.

TABLE I: Parameter settings of the proposed method.

Parameter	**Value/Type**
Wavelet filter	Coiflets family
Scale number	5
Termination threshold for FCM	0.001
Maximum number of iterations for FCM	100
Population size	20
PSO iterations	50
c_1 and c_2 in PSO	1
weighting exponent (m)	2

Some of the state-of-the-art methods also have parameters which need tuning for an optimal performance. FCM_S1, FCM_S2 and EnFCM need α to be tuned, and FGFCM, FGFCM_S1, and FGFCM_S2 need λ_g and λ_s to be tuned. As presented in [11], the best performance of these methods is guaranteed given the values $\alpha = 1.8$, $\lambda_s = 3$, and $\lambda_g = 6$. To keep the comparison fair, the surrounding window in all the comparison methods is set to 7×7 pixels. This window has been used in all the them to collect information from neighbor pixels, build a feature, and then attribute it to the pixel under consideration.

C. Statistical Significance Test

To analyze the non-deterministic behavior of PSO in our scheme, a pair-wise statistical significance test is performed. For this, the Wilconxon test with the significance level of 0.05 is selected. For more information about this test, please refer to [32]. Our algorithm runs 30 times independently on each image, and the results in the form of SA values are compared with other methods using the test. If the p-value (the probability of observing a test statistic as or more extreme than the observed value under the null hypothesis) is greater than the significance level, the pair-wise comparison is not significantly different. Otherwise, one method is significantly better than the other.

V. Results and Discussion

For each of the Synthetic and Berkeley images, there are eight different noise levels. This means there are 40 noisy test images for each dataset (80 test images in total). We name each sample noisy image an "*instance*" in this paper. In the following two sub-sections the results for each dataset is discussed separately.

A. Synthetic Dataset

In this dataset, we first consider a pair-wise comparison of the proposed method with others. A quick analysis of the results from table II and Wilconxon test shows that our method is completely (in all 40 instances) significantly better than FCM_S1, FCM_S2, EnFCM, FGFCM, FGFCM_S1, and FGFCM_S2. In comparison with FLICM our method still possesses 36 out of 40 significantly better performances. There are only three instances that FLICM has significantly better performances than the proposed method, and they are all on low noise variance of 10% for images *S*2, *S*3, and *S*4. There is also one instance (*S*4, variance = 80%) that the proposed method is not significantly different from FLICM.

To determine the overall best performance, and the first-two best performers for an instance, we do another analysis by sorting the segmentation accuracy of all the algorithms for that instance. This reveals that in 36 (out of 40) instances the best performer is the proposed method, in three instances FLICM is the best performer, and in one instance either the proposed method or FLICM is the best performer. This is the case that the p value is greater than the significance level. When considering the second-best performers, it becomes evident that our method does second-best in three instances. These three instances are the ones that FLICM has a better performance than ours. Equivalently, our method always does either best or second-best, and never worse. In this manner, methods that possess the highest number of second-best performances are FGFCM_S1 with 25, FLICM with nine, and FCM_S1, FCM_S2, EnFCM, and FGFCM with no second-best performances. This means that the latter four methods do not have any place among the first-two best performances.

B. Berkeley Dataset

For this dataset, again, with respect to the SA values provided in table III and the Wilconxon significance test, our method always does significantly better than FCM_S1, FCM_S2, EnFCM, FGFCM, and FGFCM_S1 in all the 40 instances. Pair-wise comparison to FGFCM_S2 and FLICM indicates that the proposed method is doing significantly better in 39 and 28 instances (out of 40) respectively. Eight out of the 12 instances that FLICM performs better than ours belong to image 167062.

When sorting out all the performances of all the algorithms for each instance, a quick analysis shows that our method does the best in 27 out of 40 instances, and second-best in a further 12 instances. This means that our method does the best or second-best in 39 out of 40 instances in this dataset. In a performance-decreasing manner, the rest of the algorithms perform as follows: FLICM has 12 bests and none second-best, FGFCM_S2 has one best and three second-bests, FGFCM_S1 has none best and 25 second-bests, and FCM_S1, FCM_S2, EnFCM, and FGFCM do not have any place among the first-two best performers. Another interesting point from table III is the unusual behavior of FLICM on some of the instances with unexpectedly low SA value. We will show in qualitative comparison that these are the cases that FLICM completely

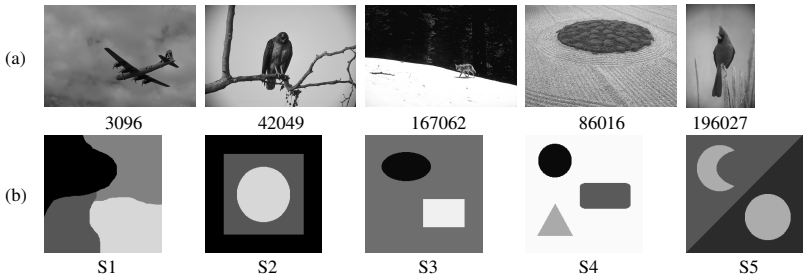

Fig. 3: Original test images from the Synthetic dataset, row (a), and Berkeley dataset, row (b).

TABLE II: SA values for the Synthetic dataset. The bold number indicates the best performance for each instance.

		Algorithm							
Img.	Vol.	FCMS1	FCMS2	EnFCM	FGFCM	FGFCMS1	FGFCMS2	FLICM	Ours
S1	10%	88.98	89.86	88.98	93.12	94.33	93.01	95.90	**97.06± 0.03**
	20%	79.41	82.85	78.95	86.22	89.66	87.22	88.04	**95.94± 0.05**
	30%	71.62	78.14	71.44	79.86	85.99	81.37	58.15	**95.46± 0.09**
	40%	67.16	74.94	67.10	75.31	82.15	77.10	44.95	**94.28± 0.10**
	50%	62.77	71.79	63.34	71.38	78.93	72.83	43.12	**94.07± 0.07**
	60%	59.78	70.42	60.64	67.94	76.36	72.67	29.27	**94.17± 0.10**
	70%	57.25	68.61	58.12	64.82	73.33	70.26	44.69	**93.19± 0.14**
	80%	55.29	66.27	56.10	62.87	69.89	67.67	30.49	**92.70± 0.04**
S2	10%	97.85	98.41	97.89	99.11	99.02	98.73	**99.18**	99.12± 0.01
	20%	92.26	95.05	92.42	96.51	97.85	96.98	97.35	**98.67± 0.03**
	30%	87.25	91.49	87.72	93.58	96.51	94.87	96.28	**98.36± 0.03**
	40%	81.72	89.21	82.85	89.11	93.49	92.02	74.52	**98.13± 0.01**
	50%	76.60	86.52	78.22	85.39	91.32	89.71	82.32	**97.64± 0.05**
	60%	74.44	85.53	76.40	83.65	90.05	88.70	74.51	**97.38± 0.01**
	70%	71.04	83.49	73.47	80.16	86.40	86.54	73.24	**97.68± 0.03**
	80%	68.52	81.58	71.02	77.76	85.56	85.59	73.89	**97.18± 0.02**
S3	10%	81.10	93.30	96.04	97.68	97.25	97.15	**99.65**	99.61± 0.00
	20%	67.89	76.50	69.33	88.37	95.48	94.37	99.19	**99.33± 0.01**
	30%	52.89	71.85	64.92	76.71	90.76	88.78	98.63	**98.92± 0.04**
	40%	45.92	67.07	60.81	72.89	86.83	84.82	65.52	**98.73± 0.02**
	50%	41.31	62.38	57.00	69.78	80.65	78.62	55.60	**98.54± 0.06**
	60%	38.72	61.55	54.03	68.78	80.23	77.18	54.36	**98.56± 0.02**
	70%	36.99	59.21	51.58	63.26	78.07	72.38	51.58	**97.79± 0.03**
	80%	34.49	58.54	49.69	62.40	75.42	70.59	45.22	**97.96± 0.08**
S4	10%	72.59	77.48	85.28	93.80	92.25	93.70	**98.16**	96.49± 0.01
	20%	54.42	67.71	72.10	72.65	84.55	82.02	92.41	**95.16± 0.08**
	30%	51.00	60.31	66.59	65.40	65.40	75.39	82.16	**93.93± 0.04**
	40%	49.36	58.30	61.76	62.01	60.43	76.61	81.68	**93.21± 0.03**
	50%	48.69	55.94	53.88	57.90	57.28	72.07	81.86	**91.89± 0.04**
	60%	48.82	54.17	50.62	56.55	56.25	70.21	88.39	**90.13± 0.32**
	70%	48.04	54.01	48.08	51.60	54.57	68.73	88.55	**90.99± 0.15**
	80%	47.76	52.40	47.51	47.01	50.01	68.26	85.70	81.70±10.08
S5	10%	85.62	86.90	85.54	90.31	93.15	90.68	57.80	**96.84± 0.09**
	20%	75.55	79.95	76.33	82.99	88.01	84.38	58.73	**95.06± 0.07**
	30%	67.21	74.05	69.03	76.47	82.39	78.03	58.25	**93.96± 0.11**
	40%	62.39	70.96	64.81	72.43	78.87	74.89	59.96	**93.09± 0.06**
	50%	57.20	66.68	60.11	67.50	73.84	70.19	58.19	**90.54± 0.13**
	60%	54.73	65.21	57.89	65.19	71.62	68.06	39.66	**90.98± 0.15**
	70%	52.90	63.78	56.20	63.36	69.29	66.56	58.90	**89.99± 0.06**
	80%	51.73	62.83	55.17	62.18	68.06	65.67	39.33	**88.04± 0.12**

TABLE III: SA values for the Berkeley dataset. The bold number indicates the best performance for each instance.

		Algorithm							
Img.	Vol.	FCMS1	FCMS2	EnFCM	FGFCM	FGFCMS1	FGFCMS2	FLICM	Ours
3096	10%	64.18	67.18	68.78	76.26	82.71	**84.41**	6.13	83.82±0.10
	20%	58.73	62.27	59.99	65.92	72.80	74.09	6.13	**79.88±0.01**
	30%	57.00	60.56	57.54	62.73	69.95	69.36	6.13	**76.67±0.03**
	40%	55.98	59.85	56.24	61.52	67.04	67.70	6.13	**82.67±0.03**
	50%	54.96	58.69	54.72	59.88	65.35	63.74	6.13	**84.33±0.01**
	60%	54.72	58.55	54.61	58.14	64.50	63.61	6.13	**76.72±0.04**
	70%	54.45	58.53	54.12	57.79	64.24	63.45	6.13	**80.44±0.07**
	80%	53.85	57.73	53.35	56.81	63.13	61.76	6.13	**80.48±0.04**
42049	10%	93.07	93.43	93.46	94.12	93.62	93.80	**95.21**	94.65±0.02
	20%	89.00	91.02	90.77	92.86	92.70	92.47	**94.16**	93.35±0.09
	30%	83.74	88.65	86.63	91.37	92.05	91.43	90.16	**92.75±0.08**
	40%	78.72	86.03	81.48	88.65	91.12	90.18	19.09	**92.27±0.04**
	50%	75.59	84.42	77.67	86.91	90.21	89.21	19.09	**91.97±1.37**
	60%	73.31	82.63	74.97	84.17	88.95	87.88	19.09	**91.17±0.11**
	70%	71.37	80.71	72.17	81.81	87.78	85.65	19.09	**91.93±0.14**
	80%	69.59	78.55	70.66	78.60	85.10	82.15	19.09	**89.84±0.23**
167062	10%	79.13	79.77	85.49	98.00	97.27	81.84	**99.06**	98.47±0.01
	20%	77.40	79.05	82.38	79.87	96.99	80.22	**99.15**	98.18±0.00
	30%	76.64	78.56	81.45	77.91	75.23	80.17	**99.20**	97.84±0.01
	40%	76.34	78.54	79.67	77.16	74.34	80.76	**99.37**	97.62±0.01
	50%	75.61	77.82	78.59	77.16	73.22	80.61	**99.19**	97.60±0.00
	60%	74.67	77.25	76.91	76.09	72.84	80.73	**99.21**	97.56±0.01
	70%	74.00	76.78	75.50	74.68	72.52	81.54	**98.94**	97.21±0.01
	80%	72.48	75.46	73.47	74.45	70.99	79.74	**98.85**	97.13±0.00
86016	10%	86.19	87.21	89.17	92.69	94.10	93.23	**99.12**	98.47±0.02
	20%	77.12	81.05	79.43	86.77	91.36	89.22	16.36	**97.81±0.01**
	30%	72.44	77.88	74.32	82.22	87.90	85.65	16.36	**97.43±0.02**
	40%	69.06	74.50	70.22	77.56	84.35	81.36	16.36	**98.31±0.04**
	50%	67.19	73.21	68.18	74.54	82.43	78.67	16.36	**97.78±0.01**
	60%	65.87	72.26	66.18	73.57	80.89	76.95	16.36	**97.81±0.00**
	70%	64.06	70.43	64.69	70.91	76.82	74.56	16.36	**96.12±0.15**
	80%	63.14	70.11	63.54	69.68	75.53	74.11	16.36	**95.89±0.04**
196027	10%	73.29	74.95	76.09	78.74	79.61	80.24	**91.09**	79.15±0.25
	20%	67.30	70.06	68.85	72.99	76.45	75.71	11.57	**76.84±0.03**
	30%	64.64	68.19	65.46	70.20	74.40	73.88	11.57	**77.78±0.02**
	40%	63.04	66.91	63.80	68.99	73.69	71.80	11.57	**78.54±0.41**
	50%	61.68	66.14	61.97	67.30	72.35	70.24	11.57	**80.08±0.16**
	60%	60.57	65.28	60.76	65.29	70.37	68.88	11.57	**76.52±0.12**
	70%	59.69	64.07	60.36	64.67	68.43	67.26	11.57	**74.19±0.06**
	80%	59.12	64.22	59.52	64.17	69.59	67.50	11.57	**75.95±0.04**

misses one or some of the components of the image in final segmentation results.

C. More Discussions

To further analyze the effect of noise volume variation on SA value, we conduct another analysis to measure the SA variance of each method on each of the ten test images from the two datasets while the noise level ranges from 10% to 80%, and then compare the results across all the methods. Table IV provides such a comparison. The table shows the SA variance of each method on each image with the minimum variance in bold. Our method has the minimum variance in nine out of ten cases. This indicates than even though the noise volume has a large diversity, regardless of the segmentation accuracy, the proposed method produces the most consistent results.

To qualitatively compare the segmentation results of our method with other methods, Fig. 4 provides a few samples from the overall 80 noisy images, and the corresponding segmentation results of all methods. The first three columns show S1, S4, and S5 from the Synthetic dataset with noise variance of 70%, 50%, and 10% respectively. The next three columns are images 3096, 167062, and 196027 from the

TABLE IV: The effect of variation of the noise level on SA variance.

Image	3096	42049	167062	86016	196027	S1	S2	S3	S4	S5
FCMS_1	11.53	72.93	4.31	60.52	22.47	136.53	109.62	275.01	69.96	145.28
FCMS_2	9.54	26.29	1.90	34.88	13.16	62.82	33.57	137.57	73.17	73.22
EnFCM	25.68	73.58	15.31	76.00	30.99	126.83	90.17	223.45	178.76	115.97
FGFCM	40.32	30.23	59.48	65.69	24.43	113.07	60.00	151.84	214.37	101.64
FGFCMS_1	42.47	7.95	124.33	43.83	13.97	69.47	25.85	67.87	230.72	83.19
FGFCMS_2	57.60	14.53	0.49	49.38	20.11	77.69	23.50	98.03	73.11	81.74
FLICM	–	1472.33	**0.03**	856.00	790.32	626.00	137.19	566.31	33.84	78.96
Ours	**8.52**	**2.05**	0.21	**0.91**	**3.60**	**2.11**	**0.45**	**0.38**	**20.74**	**8.57**

Berkeley dataset with noise variance of 80%, 40%, and 30% respectively. The last row shows how FLICM completely misses one or more number of regions in the final segmentation results.

VI. Conclusions

A new noisy image segmentation was proposed in this paper. The method utilizes wavelet thresholded coefficients, in which the optimal values of thresholds were determined using PSO. FCM was applied as a fitness metric in the PSO search, also as the segmentation algorithm. Unlike the other FCM-based noisy image segmentation methods, the proposed algorithm looks at the problem from feature manipulation point of view. To abbreviate the distinctive properties of the new method, we mention three main points. First, it shows considerably good performance on severely noisy images, second, it does not need parameter-tuning for different noise levels, and third, it produces considerably stable results even when noise volume has a large variation. Future work will explore the potential of the proposed method on other types of noise.

References

[1] J.-Y. Zhang, W. Zhang, Z.-W. Yang, and G. Tian, "A novel algorithm for fast compression and reconstruction of infrared thermographic sequence based on image segmentation," *Infrared Physics and Technology*, vol. 67, no. 0, pp. 296–305, 2014.

[2] Y. Kang, K. Yamaguchi, T. Naito, and Y. Ninomiya, "Multiband image segmentation and object recognition for understanding road scenes," *Intelligent Transportation Systems, IEEE Transactions on*, vol. 12, no. 4, pp. 1423–1433, 2011.

[3] T. Mahalingam and M. Mahalakshmi, "Vision based moving object tracking through enhanced color image segmentation using haar classifiers," in *Proceedings of the 2nd International Conference on Trendz in Information Sciences and Computing, TISC-2010*, 2010, pp. 253–260.

[4] E. AntúNez, R. Marfil, J. P. Bandera, and A. Bandera, "Part-based object detection into a hierarchy of image segmentations combining color and topology," *Pattern Recogn. Lett.*, vol. 34, no. 7, pp. 744–753, may 2013.

[5] X. Tian, L. Jiao, and X. Zhang, "A clustering algorithm with optimized multiscale spatial texture information: application to SAR image segmentation," *International Journal of Remote Sensing*, vol. 34, no. 4, pp. 1111–1126, 2013.

[6] B. Banerjee, S. Varma, K. Buddhiraju, and L. Eeti, "Unsupervised multi-spectral satellite image segmentation combining modified mean-shift and a new minimum spanning tree based clustering technique," *Selected Topics in Applied Earth Observations and Remote Sensing, IEEE Journal of*, vol. 7, no. 3, pp. 888–894, March 2014.

[7] M. Ahmed, S. Yamany, N. Mohamed, and A. Farag, "A Modified Fuzzy C-Means Algorithm for MRI Bias Field Estimation and Adaptive Segmentation," ser. Lecture Notes in Computer Science. Springer Berlin Heidelberg, 1999, vol. 1679, pp. 72–81.

[8] S. Chen and D. Zhang, "Robust image segmentation using fcm with spatial constraints based on new kernel-induced distance measure," *Systems, Man, and Cybernetics, Part B: Cybernetics, IEEE Transactions on*, vol. 34, no. 4, pp. 1907–1916, Aug 2004.

[9] L. Szilagyi, Z. Benyo, S. Szilagyi, and H. Adam, "Mr brain image segmentation using an enhanced fuzzy c-means algorithm," in *Engineering in Medicine and Biology Society, 2003. Proceedings of the 25th Annual International Conference of the IEEE*, vol. 1, Sept 2003, pp. 724–726 Vol.1.

[10] W. Cai, S. Chen, and D. Zhang, "Fast and robust fuzzy c-means clustering algorithms incorporating local information for image segmentation," *Pattern Recognition*, vol. 40, no. 3, pp. 825–838, 2007.

[11] S. Krinidis and V. Chatzis, "A robust fuzzy local information c-means clustering algorithm," *Image Processing, IEEE Transactions on*, vol. 19, no. 5, pp. 1328–1337, May 2010.

[12] X. Wang, X. Lin, and Z. Yuan, "An edge sensing fuzzy local information c-means clustering algorithm for image segmentation," ser. Lecture Notes in Computer Science. Springer International Publishing, 2014, vol. 8589, pp. 230–240.

[13] R. R. Z. M. Mirghasemi, S., "A new modification of fuzzy c-means via particle swarm optimization for noisy image segmentation," in *Proceedings of the Second Australasian Conference, ACALCI 2016, Canberra, ACT, Australia*, 2016, pp. 147–159.

[14] S. Mirghasemi, R. Rayudu, and M. Zhang, "A heuristic solution for noisy image segmentation using particle swarm optimization and fuzzy clustering," in *Proceedings of the 7th International Joint Conference on Computational Intelligence*, 2015, pp. 17–27.

[15] S. Mirghasemi, H. Sadoghi Yazdi, and M. Lotfizad, "A target-based color space for sea target detection," *Applied Intelligence*, vol. 36, no. 4, pp. 960–978, 2012.

[16] M. Setayesh, M. Zhang, and M. Johnston, "A novel particle swarm optimisation approach to detecting continuous, thin and smooth edges in noisy images ," *Information Sciences*, vol. 246, pp. 28–51, 2013.

[17] J. C. Dunn, "A Fuzzy Relative of the ISODATA Process and Its Use in Detecting Compact Well-Separated Clusters," *Journal of Cybernetics*, vol. 3, no. 3, pp. 32–57, 1973.

[18] R. Hathaway, J. Bezdek, and Y. Hu, "Generalized fuzzy c-means clustering strategies using lp norm distances," *Fuzzy Systems, IEEE Transactions on*, vol. 8, no. 5, pp. 576–582, Oct 2000.

[19] J. Feng, L. Jiao, X. Zhang, M. Gong, and T. Sun, "Robust non-local fuzzy c-means algorithm with edge preservation for {SAR} image segmentation ," *Signal Processing*, vol. 93, no. 2, pp. 487–499, 2013.

[20] S. G. Mallat, "A theory for multiresolution signal decomposition: The wavelet representation," *IEEE Trans. Pattern Anal. Mach. Intell.*, vol. 11, no. 7, pp. 674–693, Jul. 1989.

[21] D. L. Donoho, "De-noising by soft-thresholding," *IEEE Transactions on Information Theory*, vol. 41, no. 3, pp. 613–627, May 1995.

[22] R. Eberhart and J. Kennedy, "A new optimizer using particle swarm theory," in *Micro Machine and Human Science, 1995. MHS '95., Proceedings of the Sixth International Symposium on*, 1995, pp. 39–43.

[23] J. Kennedy and R. Eberhart, "Particle swarm optimization," in *Neural Networks, 1995. Proceedings., IEEE International Conference on*, vol. 4, 1995, pp. 1942–1948 vol.4.

[24] A. Benaichouche, H. Oulhadj, and P. Siarry, "Improved spatial fuzzy c-means clustering for image segmentation using {PSO} initialization, Mahalanobis distance and post-segmentation correction," *Digital Signal Processing*, vol. 23, no. 5, pp. 1390–1400, 2013.

[25] D. Tran, Z. Wu, and V. Tran, "Fast Generalized Fuzzy C-means Using Particle Swarm Optimization for Image Segmentation," in *Neural Information Processing*, ser. Lecture Notes in Computer Science, C. Loo, K. Yap, K. Wong, A. Teoh, and K. Huang, Eds. Springer International Publishing, 2014, vol. 8835, pp. 263–270.

[26] Q. Zhang, C. Huang, C. Li, L. Yang, and W. Wang, "Ultrasound image segmentation based on multi-scale fuzzy c-means and particle swarm

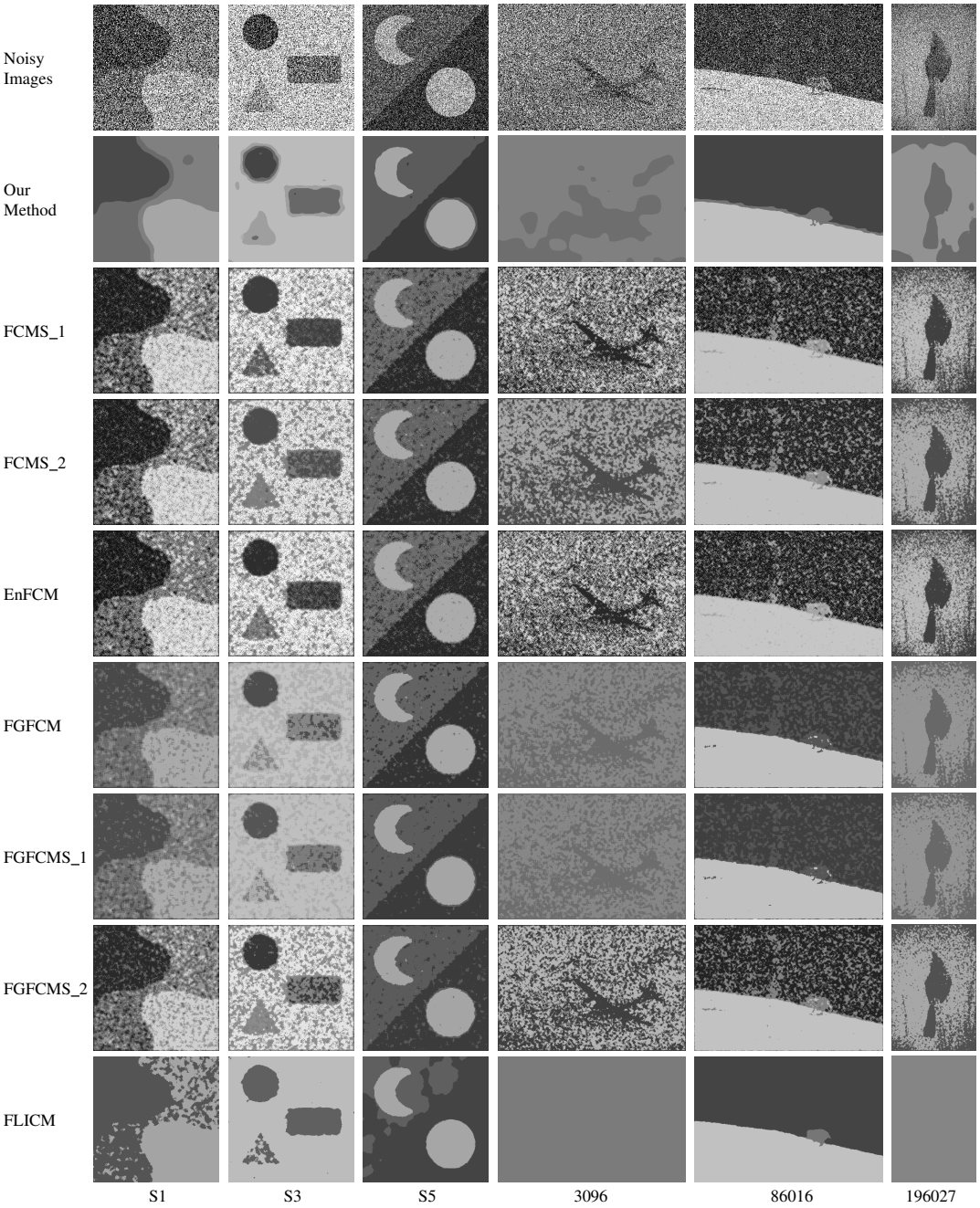

Fig. 4: Qualitative comparison of the proposed method with FCM_S1, FCM_S2, EnFCM, FGFCM_S1, FGFCM_S2, FGFCM, and FLICM on some instances from the Synthetic and Berkeley datasets. S1, S4, S5, 3096, 167062, and 196027 are corrupted by Gaussian noise with variance of 70%, 50%, 10%, 80%, 40%, and 30% respectively.

optimization," in *Information Science and Control Engineering 2012 (ICISCE 2012), IET International Conference on*, Dec 2012, pp. 1–5.

[27] X. Tian, L. Jiao, L. Yi, K. Guo, and X. Zhang, "The image segmentation based on optimized spatial feature of superpixel ," *Journal of Visual Communication and Image Representation*, vol. 26, pp. 146–160, 2015.

[28] D. L. DONOHO and J. M. JOHNSTONE, "Ideal spatial adaptation by wavelet shrinkage," *Biometrika*, vol. 81, no. 3, pp. 425–455, 1994.

[29] H.-Y. Gao, "Wavelet shrinkage denoising using the non-negative garrote," *Journal of Computational and Graphical Statistics*, vol. 7, no. 4, pp. 469–488, 1998.

[30] A. Bhandari, M. Gadde, A. Kumar, and G. Singh, "Comparative analysis of different wavelet filters for low contrast and brightness enhancement of multispectral remote sensing images," in *Machine Vision and Image Processing (MVIP), 2012 International Conference on*, Dec 2012, pp. 81–86.

[31] D. Martin, C. Fowlkes, D. Tal, and J. Malik, "A database of human segmented natural images and its application to evaluating segmentation algorithms and measuring ecological statistics," in *Proc. 8th Int'l Conf. Computer Vision*, vol. 2, July 2001, pp. 416–423.

[32] F. Wilcoxon, "Individual comparisons by ranking methods," *Biometrics Bulletin*, vol. 1, no. 6, pp. 80–83, 1945.